A New Tool for Digital Alignment in Virtual Anthropology

ANTONIO PROFICO,[1*] COSTANTINO BUZI,[1] CHRISTOPHER DAVIS,[2] MARINA MELCHIONNA,[3] ALESSIO VENEZIANO,[4] PASQUALE RAIA,[3] AND GIORGIO MANZI[1]

[1]Dipartimento di Biologia Ambientale, Sapienza Università di Roma, Rome, Italy
[2]Department of Anthropology, University of Texas at Austin, Austin, Texas
[3]Dipartimento di Scienze della Terra, dell'Ambiente e delle Risorse, Università di Napoli Federico II, Naples, Italy
[4]School of Natural Sciences and Psychology, John Moores University, Liverpool, UK

ABSTRACT

The study of the fossil record is fundamental to understand the evolution of traits. Because fossil remains are often fragmented and/or deformed by taphonomic processes, a preliminary realignment of their constituent parts is often necessary to properly interpret their shapes. In virtual anthropology, these procedures are carried out using digital models of the remains. We present a new semi-automatic alignment R software, Digital Tool for Alignment (DTA), which uses the shape information contained in a reference sample to find the best alignment solution for the disarticulated regions. We tested DTA on three different case-studies: (1) a sample of 14 primate species including both male and female individuals, (2) a simulated, disarticulated skull of *Homo sapiens*, and (3) a real disarticulated human fossil specimen, Amud 1 (*Homo neanderthalensis*). In the first case study, we simulated disarticulation directly on digital models of the primate skulls and tested alignment quality as a function of phylogenetic proximity, sex, and body size. In the second, we compared DTA to manual alignments conducted for the same digital models. Finally, we performed DTA on a real-world case study. We found that phylogenetic proximity provides is the most important factor for alignment efficiency. However, sex and allometric effects might also be important and should therefore be taken into account at selecting reference models for alignments. DTA performs at least as well as manual alignments. Yet, as compared to manual procedures, it is faster, requires no prior anatomical knowledge and expertise and allows indefinite manipulation of the fossil items. Anat Rec, 302:1104–1115, 2019. © 2019 Wiley Periodicals, Inc.

Key words: geometric morphometrics; fossil; primates; R; virtual restoration; *Homo neanderthalensis*

Fossil remains often appear badly deformed by biostratinomic and taphonomic processes (Hughes and Jell, 1992; Arbour and Currie, 2012; Schlager et al., 2018) which usually result in major cracks, missing portions, or alteration of the biological symmetry (Ogihara et al., 2006; Arbour and Brown, 2013; Di Vincenzo et al., 2017). This lack of information can

Additional Supporting Information may be found in the online version of this article.

Abbreviations: AM = aligned model; DM = disarticulate model; DTA = Digital Alignment Tool; GPA = generalized Procrustes analysis; RM = reference model; SM = starting model

*Correspondence to: Antonio Profico, Dipartimento di Biologia Ambientale, Sapienza Università di Roma, Piazzale Aldo Moro 00187, 5, Rome, Italy. Fax: +39 0649912690

E-mail: antonio.profico@uniroma1.it

Received 12 March 2018; Revised 8 September 2018; Accepted 26 September 2018.

DOI: 10.1002/ar.24077

Published online 7 February 2019 in Wiley Online Library (wileyonlinelibrary.com).

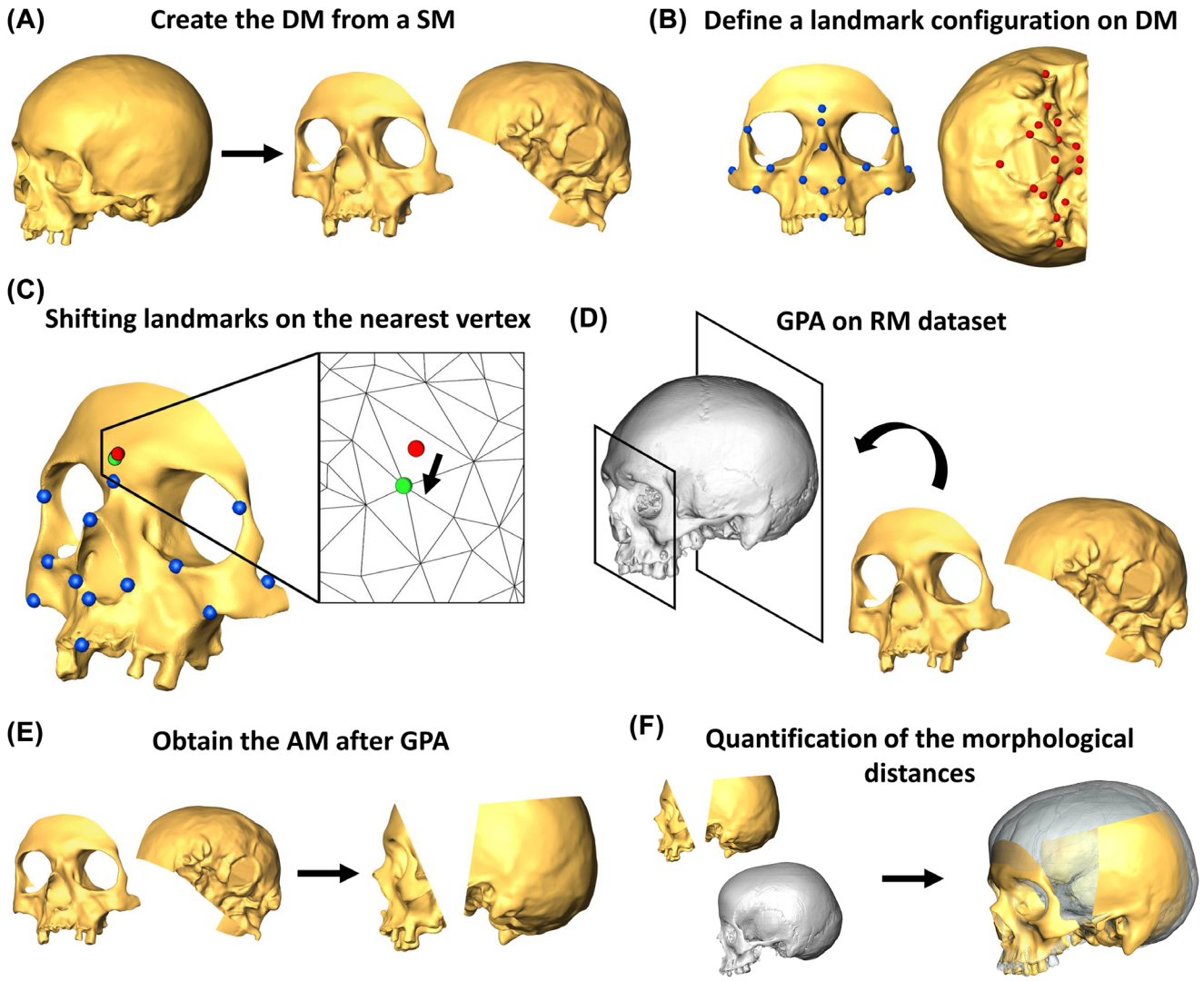

Fig. 1. DTA methodology explained step by step. (**A**) Definition of the disarticulated model (DM) from a starting model (SM). (**B**) Definition of a landmark configuration on both face complex and cranial base of DM. (**C**) Shifting landmarks of DM model (in red) on the nearest vertex of the mesh (in green). (**D**) Compute a General Procrustes Analysis (GPA) of the facial complex and the cranial base on each reference model (RM). (**E**) Alignment of the two halves of the DM after the GPA. (**F**) Quantification of the morphological distance between the aligned configuration and the reference model dataset. Abbreviations: DTA = Digital Alignment Tool; DM = disarticulated model; L set = landmark set; RM = reference model; GPA = generalized Procrustes analysis.

now be recovered by applying virtual reconstruction procedures, which take advantage of software implementations to perform the restoration of the digital versions of fossil remains. Three-dimensional imaging techniques further allow substituting manual intervention with virtual protocols (Shipman, 1981; Lyman, 1994; Profico et al., 2018a), which guarantee the physical preservation of the fossil specimen and avoids potential alterations of its original shape as introduced by the manual operator. Missing morphological information can be digitally recovered either by using the preserved shape information on the deficient specimen (e.g., by exploiting biological symmetry) or through the use of a 3D comparative sample of phylogenetically close species, conspecifics, or individuals of the same sex (Gunz et al., 2009). Several case-studies are reported in the literature (Zollikofer et al., 2005; Benazzi et al., 2014; Amano et al., 2015; Di Vincenzo et al., 2017), and the use of virtual reconstructions is now becoming commonplace. Unfortunately, the efficiency of the virtual reconstruction is rarely quantified (e.g., Ogihara et al., 2006; Tallman et al., 2014; Schlager et al., 2018).

Herein, we present the Digital Tool for Alignment (DTA), a new landmark-based procedure to align portions of the same (broken) skull. The procedure simulates the manual and/or landmark-based alignment commonly used in virtual anthropology studies and allows the digital restoration of fragmented remains for which anatomical/geometrical points are still recognizable, even for regions which are not in anatomical continuity.

This work is articulated in three parts. First, we assessed the influence of (1) phylogenetic distance, (2) sex, and (3) body size on DTA performance. To this aim, we analyzed a large sample of 14 different primate species, of both sexes, for a total of 131 individuals.

Second, we compared digital alignments to manual alignments by using a digital model of a single *Homo sapiens* skull as a target, taking advantage of help from expert operators in the field of virtual anthropology and digital restoration.

Lastly, we performed DTA on the Amud 1 cranial material. Amud 1 is a Neanderthal specimen composed by two anatomical regions not in continuity: the maxillary region and the neurocranium including some elements of the facial complex.

Both the R code and a selected material are fully available as parts of the R-package Arothron (Profico et al., 2018b).

MATERIALS AND METHODS

The Digital Alignment Tool

DTA is a landmark-based methodology, written in R, which allows the user to align two portions of a 3D mesh (here to fore the disarticulated model, DM) by using a reference sample or model (RM) for comparison (Fig. 1A). To run DTA, a set of anatomical landmarks is defined first on two separated portions of the DM (Fig. 1B). Each point of each landmark set is then moved to the nearest vertex of the mesh triangles (Fig. 1C). This way, each landmark is identified by a number corresponding to a row of the vertex matrix of the mesh, and its position is tracked on the 3D models moved in the Cartesian coordinate system. The second step is the alignment via Generalized Procrustes Analysis (GPA) of each part of the DM (Fig. 1D) on each RM of the comparative sample, where the same landmark configuration used for the DM has been previously defined. Steps *c* and *d* make it possible to define the landmark set on both the DM and the aligned model (AM) (Fig. 1E).

The items of the reference sample are previously scaled to the mean of the single scale factors calculated for each half of the DM, separately, and symmetrized *via* reflection and relabeling, thereby producing a perfectly symmetrical, bilateral, and scaled landmark configuration (to avoid alignment errors introduced by asymmetry).

The third step consists of quantifying the morphological distances between each part of the DM and the corresponding landmark configurations on each item in the RM sample (Fig. 1F). DTA allows calculation of the morphological distance using either one of two different metrics: the total displacement (Euclidean distance) and/or the Procrustes distance.

Then, the single specimen in the reference set with the lowest morphological distance to DM is selected as the best RM for the digital alignment to reconstruct the integral shape of the target (Fig. 1F). A complete list of abbreviation used here is reported in Table 1.

TABLE 1. Models nomenclature. Labels of the models with abbreviation and definition used in the text

Label model	Abbreviation	Definition
Starting model	SM	The SM is the mesh of the specimen used as case study.
Disarticulate model	DM	The SM cut in two different parts. Each part is translated in the Cartesian coordinate system losing the starting spatial orientation.
Reference model	RM	The RM is the model used as reference to align the two portions of the DM through two different Procrustes Fittings: each one performed on one of the two halves of the DM.
Aligned model	AM	Merge of the two halves of the DM after the aligning via Procrustes fitting on the selected RM.

Datasets

Case study 1. Primate sample. We collected a sample of 131 sexed, adult skulls of 14 different primate species. The specimens belong to the virtual collections of the Smithsonian Institution (www.vertebrates.si.edu, Washington), the Kyoto University Primate Museum (www.dmm.pri.kyoto-u.ac.jo, KUPRI, Kyoto, Japan), the anthropological museum, "G. Sergi" of the Sapienza University of Rome (Italy) and Morphosource (www.morphosource.org) (Supplementary Information Table S1). On each specimen, we recorded 61 three-dimensional landmarks (Fig. 2, Supplementary Information Table S2). The 3D coordinates were acquired using the software Amira® (version 5.4.5, Visualization Sciences Group, ©2013; https://www.fei.com/software/amira-for-life-sciences/).

For each of the 14 species in the sample, we built two separate DMs choosing both a female and a male specimen at random. The process starts by dividing the 3D model in two inequal halves, along a plane passing through three points, which were chosen to simulate a fracture separating the face from the neurocranium: (1) the middle point, along the midsagittal plane, between the spheno-occipital suture and the two sphenoidal spines lines; the middle point along the (2) right and (3) left frontozygomatic suture. The two halves were then randomly translated in the *xyz* Cartesian system to change their original spatial position.

We applied DTA to each of the 28 DMs (one male and one female per species) using the remaining 130 specimens as the reference sample. This leads to a total amount of 3,640 alignments (28 disarticulated individuals times 130 individuals in each reference sample set).

Case study 2.* Homo sapiens *skull. The specimen used as a target for all the alignments is a disarticulated, female modern human skull (BOL_2548) belonging to the "Bolognesi" collection preserved at the "G. Sergi" Anthropology Museum Rome (Italy) (Supplementary Information Fig. S1). BOL_2548 was restored using a comparative sample of *Homo sapiens* skulls including 32 three-dimensional landmarks acquired on 50 different modern human specimens (Fig. 3, Supplementary Information Table S3), belonging to the "G. Sergi" Anthropology Museum Rome (Italy), Oloriz collections, and NESPOS database (Supplementary Information Table S4). The 3D coordinates were acquired using the software Amira® (version 5.4.5, Visualization Sciences Group, ©2013; https://www.fei.com/software/amira-for-life-sciences/).

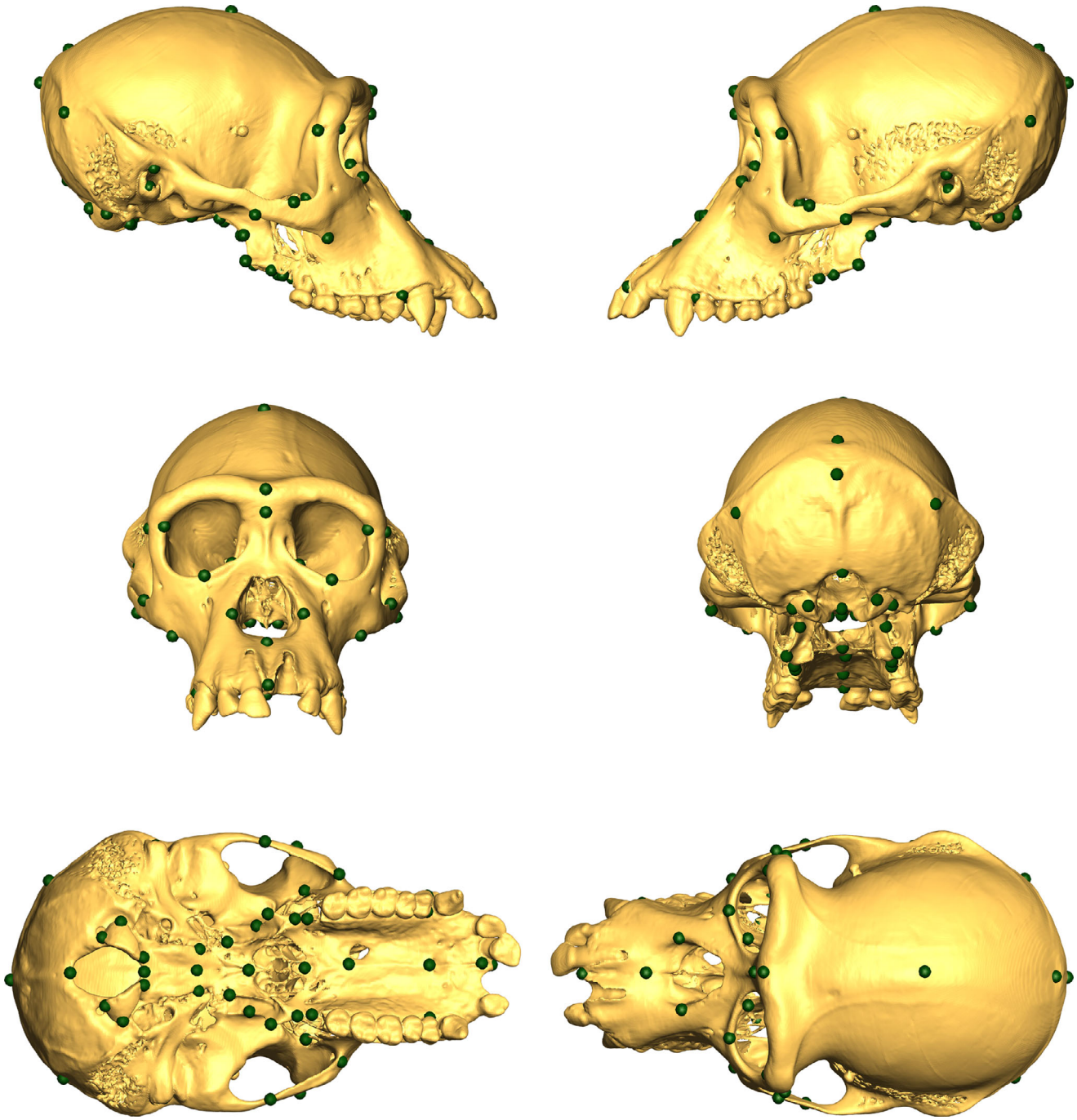

Fig. 2. Landmark configuration used in the primate case-study.

The DM consists of two portions belonging to the specimen BOL_2548, not in topological continuity, which are parts of the neurocranium and the facial complex, respectively (Supplementary Information Fig. S2). We defined a landmark configuration on each of the two halves (afterward "cranial base" and "face complex") and applied DTA using a modern human sample of 50 specimens as the reference set. We calculated the Procrustes distance between the landmark sets from the reference sample and the landmark sets of the two halves of the disarticulated model. Eventually, the specimen of the reference sample which best fit the aligned model was selected.

***Case study 3. Real-world fossil items: Amud 1* (Homo neanderthalensis).** Amud 1 is a Neanderthal skull excavated at Amud cave in Israel in 1961 (Suzuki and Takai, 1970). This specimen has undergone several different virtual reconstructions (Suzuki and Takai, 1970; Amano et al., 2015). Although the skull is severely damaged, two non-contiguous macro anatomical

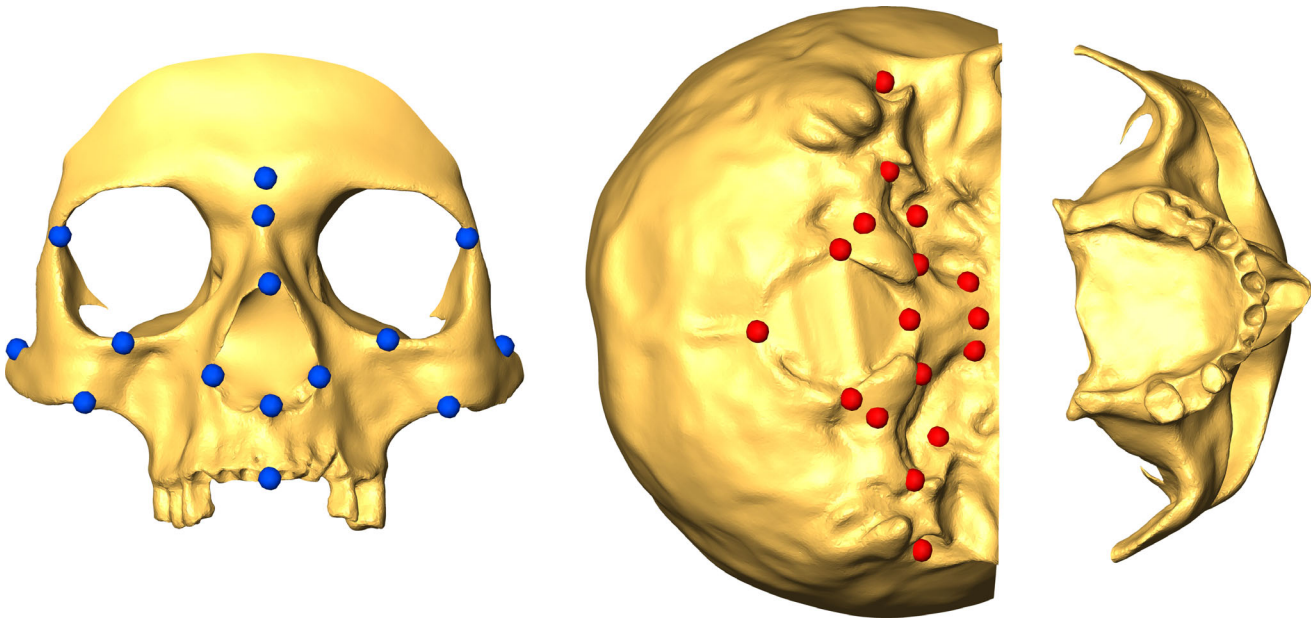

Fig. 3. The two landmark configurations shown on the "cranial base" (in red) and "face complex" (in blue) 3D models (*Homo sapiens* case-study).

regions are well-preserved: (1) the neurocranium with partial cranial base and facial complex (hereafter Amud 1a) and (2) the maxillary region (hereafter Amud 1b). We isolated the two regions of the DM (Amud 1a + Amud 1b) using the software Geomagic Studio 2014. Then, we acquired two landmark sets of 16 (Amud 1a) and 17 (Amud 1b) landmarks, respectively (Fig. 4). In addition, we defined two semi-landmark sets of 104 and 42 points on Amud 1a and Amud 1b (Fig. 4). DTA provides the option of performing the alignment by using a comparative sample and/or by using a single specimen chosen as a reference model. In the present case, we opted for the latter using Shanidar 1 and La Ferrassie I Neanderthal skulls as reference models and the restoration of Amud 1 by Suzuki (Suzuki and Takai, 1970) as the starting model (SM) used to derive the DM.

Evaluation of DTA Performance

To evaluate DTA performance, we applied ANOVA on the 3,640 alignments performed on the modern primate sample, to compare differences in Procrustes distance among groups, pooled by taxonomic status and sex, between the SM and the AM. In addition, we calculated the correlation between the Procrustes distance and two vectors representing, respectively, the phylogenetic and the centroid size distances pooled per species, using the Spearman coefficient. The phylogenetic distance was calculated as the number of nodes between the starting and the reference species. The phylogenetic tree was obtained from molecular data (available on the 10KTrees website, Arnold et al., 2010) and pruned down to the 14 OTUs analyzed here. The centroid size distance was calculated by transforming the differences in size between the starting and the reference species.

The *Homo sapiens* case study includes 51 DTAs (the DM and 50 RMs) and 11 manual alignments performed by anonymous operators who are experts in the field. We compared the results, in terms of Procrustes distance, of the two sets of alignments.

In the case of Amud 1, four DTAs were performed, using either landmark or landmark + semi-landmark configurations, and selecting either Shanidar 1 or La Ferrassie 1 as the RM. We reported the result of our alignments (AMs) and compared them to the SM (i.e., the original reconstruction of Amud 1) by calculating the average distance between DM and AMs, in terms of the mean Euclidean distance between the vertices belonging to the DM and AM.

We supply the R code (Supplementary Information R code 1) for comparison of the performance of DTA and manual alignment. This way, the reader can manually align the disarticulated model presented here as well as repeat the *Homo sapiens* case study.

RESULTS

Primate Sample

Applying the digital alignment tool (DTA) to each of the 28 primate DMs (one male and one female individual per species) and using the remaining 130 specimens as the reference sample we obtained $28 \times 130 = 3{,}640$ alignments (Table 2). The results of the ANOVA test always returned statistically significant *P*-values associated to the same-species group (Table 3). The *P*-values for the variable "sex" are statistically significant in 21 of 28 cases (Table 3).

The phylogenetic distance and the CS values are significantly correlated (Spearmen coefficients) with the Procrustes distance between SMs and the RMs in 6 of 28 and 12 of 28 case studies, respectively (Table 4).

In 15 of the 28 cases, the smallest Procrustes distance is observed between the DM and an RM belonging to an individual of the same species as the DM. Among these, 11 times the RM individual was also the same sex as the DM individual (Table 2). This result unsurprisingly shows that individuals of the same sex and species as the DM are the best reference for alignment. However, allometric effects play a large role. Thirteen times (out of 28) the

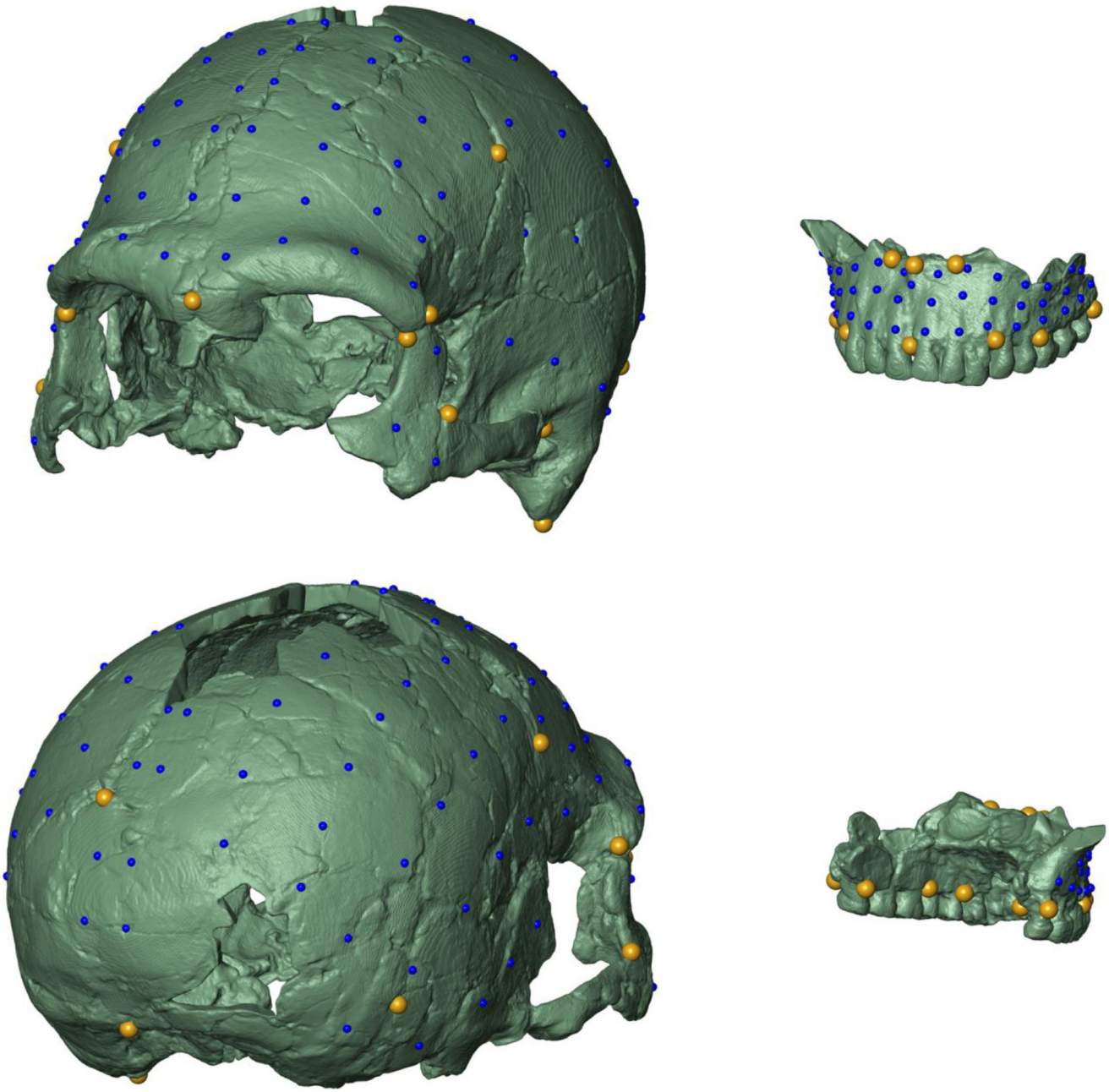

Fig. 4. Landmark (in yellow) and semi-landmark (in blue) configurations shown on the DM of Amud 1 (*Homo neanderthalensis*). Abbreviations: DM = disarticulated model.

selected RM was the same species and the closest in CS to the DM individual, which means body size is as important as sex in determining the reference model selection.

Homo sapiens. DTA applied to the female modern human disarticulated skull "BOL_2548" identifies the reference specimen "BOL_2546" (another female individual) as the morphologically closest RM (Table 5).

The Procrustes distance between the AM (built on "BOL_2546") and the SM (unbroken "2548") is equal to 0.0046. The average Procrustes distance of the manual alignments group from the starting model is twice that much, reaching 0.0110 on average (95% CI = 0.0079–0.0142). In only 2 of the 11 manual alignments, the distance between the SM and the AM is lower than the distance from the best fit found by DTA. The range of the distances between the manual alignments and the SM is bracketed from 0.0032 to 0.0175 (Figs. 5 and 6). The mean Procrustes distances between the SM and the AMs performed on the comparative sample is 0.006.

Amud 1. We applied DTA on the DM of Amud 1 using the Neanderthal specimens Shanidar 1 and La Ferrassie 1 as references. For each RM, we performed two

TABLE 2. Procrustes distances pooled by species calculated between the starting models (28 case-studies) and the reference sample

Species	Sex	*A. caraya*	*A. caraya*	*A. palliata*	*A. palliata*	*At. geoffroyi*	*At. geoffroyi*	*C. albifrons*	*C. albifrons*	*G. gorilla*	*G. gorilla*	*H. sapiens*	*H. sapiens*	*Hy. lar*	*Hy. lar*
A. caraya	F	0.00	0.01	0.00	0.01	0.01	0.01	0.01	0.01	0.04	0.05	0.03	0.03	0.01	0.01
A. caraya	M	0.06	0.03	0.07	0.06	0.09	0.08	0.13	0.12	0.24	0.31	0.20	0.22	0.10	0.08
A. palliata	F	0.01	0.02	0.01	0.01	0.02	0.02	0.02	0.02	0.10	0.13	0.07	0.08	0.02	0.02
A. palliata	M	0.06	0.13	0.04	0.09	0.06	0.07	0.07	0.07	0.38	0.45	0.29	0.32	0.07	0.09
At. geoffroyi	F	0.04	0.06	0.03	0.04	0.02	0.02	0.04	0.03	0.20	0.26	0.14	0.15	0.03	0.04
At. geoffroyi	M	0.03	0.05	0.03	0.03	0.02	0.02	0.05	0.04	0.18	0.23	0.12	0.14	0.03	0.03
C. albifrons	F	0.03	0.06	0.03	0.04	0.03	0.03	0.01	0.01	0.14	0.18	0.10	0.11	0.03	0.04
C. albifrons	M	0.02	0.04	0.02	0.03	0.02	0.02	0.01	0.01	0.11	0.14	0.07	0.08	0.02	0.02
G. gorilla	F	0.05	0.04	0.05	0.05	0.05	0.05	0.06	0.06	0.02	0.02	0.03	0.03	0.05	0.05
G. gorilla	M	0.05	0.04	0.05	0.05	0.05	0.05	0.05	0.05	0.02	0.02	0.03	0.03	0.05	0.05
H. sapiens	F	0.34	0.31	0.34	0.32	0.30	0.29	0.36	0.35	0.25	0.30	0.07	0.09	0.30	0.28
H. sapiens	M	0.23	0.20	0.23	0.22	0.21	0.21	0.25	0.24	0.13	0.18	0.06	0.05	0.21	0.20
Hy. lar	F	0.09	0.15	0.08	0.10	0.07	0.07	0.07	0.07	0.36	0.44	0.26	0.29	0.04	0.06
Hy. lar	M	0.03	0.04	0.02	0.03	0.02	0.02	0.03	0.03	0.13	0.17	0.08	0.09	0.01	0.01
M. cyclopis	F	0.01	0.01	0.01	0.01	0.01	0.01	0.01	0.01	0.03	0.05	0.02	0.03	0.01	0.01
M. cyclopis	M	0.01	0.01	0.01	0.01	0.01	0.01	0.01	0.01	0.03	0.04	0.02	0.02	0.01	0.01
P. troglodytes	F	0.27	0.21	0.28	0.25	0.26	0.26	0.33	0.32	0.14	0.21	0.16	0.17	0.27	0.24
P. troglodytes	M	0.21	0.17	0.22	0.20	0.21	0.20	0.25	0.25	0.09	0.16	0.12	0.12	0.21	0.19
Pa. hamadryas	F	0.01	0.01	0.01	0.01	0.01	0.01	0.01	0.01	0.02	0.03	0.01	0.02	0.01	0.01
Pa. hamadryas	M	0.02	0.02	0.02	0.02	0.02	0.02	0.02	0.02	0.01	0.02	0.02	0.02	0.02	0.02
Po. abelii	F	0.07	0.05	0.07	0.06	0.07	0.07	0.08	0.08	0.05	0.07	0.04	0.04	0.07	0.06
Po. abelii	M	0.10	0.08	0.10	0.09	0.10	0.10	0.12	0.11	0.04	0.05	0.07	0.07	0.10	0.09
Po. pygmaeus	F	0.33	0.27	0.34	0.31	0.33	0.32	0.41	0.40	0.15	0.20	0.23	0.23	0.34	0.30
Po. pygmaeus	M	0.34	0.28	0.35	0.32	0.34	0.33	0.40	0.39	0.15	0.17	0.23	0.23	0.34	0.31
S. syndactylus	F	0.04	0.03	0.04	0.03	0.03	0.03	0.05	0.05	0.10	0.14	0.07	0.08	0.03	0.02
S. syndactylus	M	0.03	0.03	0.03	0.03	0.03	0.03	0.05	0.05	0.11	0.15	0.07	0.08	0.03	0.02
T. gelada	F	0.07	0.06	0.07	0.06	0.07	0.06	0.09	0.08	0.12	0.18	0.09	0.10	0.07	0.06
T. gelada	M	0.02	0.01	0.02	0.02	0.02	0.02	0.02	0.02	0.02	0.03	0.02	0.02	0.02	0.02

Species	Sex	*M. cyclopis*	*M. cyclopis*	*P. troglodytes*	*P. troglodytes*	*Pa. hamadryas*	*Pa. hamadryas*	*Po. abelii*	*Po. abelii*	*Po. pygmaeus*	*Po. pygmaeus*	*S. syndactylus*	*S. syndactylus*	*T. gelada*	*T. gelada*
A. caraya	F	0.01	0.01	0.03	0.03	0.02	0.03	0.03	0.04	0.03	0.04	0.01	0.01	0.02	0.02
A. caraya	M	0.09	0.09	0.16	0.18	0.10	0.16	0.17	0.25	0.19	0.22	0.08	0.08	0.14	0.13
A. palliata	F	0.02	0.02	0.07	0.08	0.04	0.07	0.07	0.11	0.08	0.10	0.03	0.03	0.04	0.05
A. palliata	M	0.10	0.12	0.27	0.31	0.18	0.28	0.29	0.39	0.33	0.36	0.12	0.14	0.19	0.22
At. geoffroyi	F	0.04	0.05	0.13	0.15	0.08	0.14	0.15	0.22	0.17	0.19	0.05	0.06	0.09	0.11
At. geoffroyi	M	0.04	0.04	0.11	0.13	0.07	0.12	0.13	0.19	0.15	0.17	0.04	0.05	0.08	0.09
C. albifrons	F	0.04	0.05	0.10	0.11	0.06	0.10	0.11	0.15	0.12	0.13	0.05	0.05	0.06	0.08
C. albifrons	M	0.03	0.03	0.07	0.09	0.05	0.08	0.08	0.12	0.09	0.11	0.03	0.04	0.05	0.06
G. gorilla	F	0.04	0.04	0.03	0.02	0.04	0.03	0.02	0.02	0.02	0.02	0.04	0.04	0.04	0.03
G. gorilla	M	0.05	0.04	0.03	0.03	0.04	0.03	0.03	0.02	0.02	0.02	0.04	0.04	0.04	0.03
H. sapiens	F	0.27	0.25	0.19	0.20	0.25	0.28	0.22	0.29	0.25	0.28	0.25	0.25	0.33	0.27
H. sapiens	M	0.19	0.18	0.10	0.10	0.16	0.15	0.12	0.16	0.13	0.15	0.17	0.17	0.20	0.16
Hy. lar	F	0.10	0.12	0.25	0.29	0.17	0.28	0.28	0.38	0.31	0.35	0.11	0.12	0.20	0.22
Hy. lar	M	0.02	0.03	0.08	0.09	0.05	0.09	0.09	0.14	0.10	0.12	0.03	0.03	0.06	0.07
M. cyclopis	F	0.00	0.01	0.02	0.03	0.01	0.02	0.02	0.04	0.03	0.03	0.01	0.01	0.01	0.01
M. cyclopis	M	0.00	0.00	0.02	0.02	0.01	0.02	0.02	0.03	0.02	0.03	0.01	0.01	0.01	0.01
P. troglodytes	F	0.23	0.21	0.08	0.06	0.17	0.15	0.09	0.16	0.11	0.14	0.20	0.19	0.25	0.16
P. troglodytes	M	0.19	0.17	0.06	0.04	0.14	0.11	0.06	0.11	0.08	0.10	0.16	0.16	0.19	0.12
Pa. hamadryas	F	0.01	0.01	0.01	0.01	0.00	0.01	0.01	0.02	0.02	0.02	0.01	0.01	0.01	0.01
Pa. hamadryas	M	0.02	0.02	0.01	0.01	0.01	0.00	0.01	0.02	0.01	0.02	0.02	0.02	0.02	0.01
Po. abelii	F	0.06	0.05	0.02	0.02	0.04	0.04	0.02	0.05	0.03	0.04	0.05	0.05	0.06	0.04
Po. abelii	M	0.09	0.09	0.05	0.04	0.07	0.05	0.04	0.03	0.04	0.03	0.08	0.08	0.09	0.06
Po. pygmaeus	F	0.29	0.26	0.12	0.09	0.23	0.20	0.09	0.14	0.11	0.13	0.25	0.25	0.31	0.20
Po. pygmaeus	M	0.31	0.29	0.16	0.12	0.26	0.21	0.13	0.13	0.12	0.13	0.27	0.27	0.32	0.23
S. syndactylus	F	0.03	0.02	0.06	0.07	0.04	0.07	0.07	0.11	0.08	0.10	0.02	0.02	0.05	0.05
S. syndactylus	M	0.03	0.02	0.06	0.07	0.04	0.07	0.07	0.12	0.09	0.10	0.01	0.02	0.05	0.05
T. gelada	F	0.04	0.04	0.07	0.09	0.02	0.06	0.08	0.13	0.10	0.12	0.05	0.05	0.06	0.03
T. gelada	M	0.01	0.01	0.01	0.01	0.01	0.01	0.01	0.02	0.01	0.02	0.01	0.01	0.01	0.00

Abbreviations: F = female; M = male.

TABLE 3. ANOVA performed on the Primate case study. ANOVA summary (P-values) performed between the Procrustes distances (Table 2) and the categorical variables OTU (species) and Sex. The values that are statistically significant are indicated in bold

Species	SEX	OTU	SEX
Alouatta caraya	F	**0.00**	**0.00**
Alouatta caraya	M	**0.00**	**0.00**
Alouatta palliata	F	**0.00**	**0.00**
Alouatta palliata	M	**0.00**	**0.00**
Ateles geoffroyi	F	**0.00**	**0.00**
Ateles geoffroyi	M	**0.00**	**0.00**
Cebus albifrons	F	**0.00**	**0.00**
Cebus albifrons	M	**0.00**	**0.00**
Gorilla gorilla	F	**0.00**	**0.00**
Gorilla gorilla	M	**0.00**	**0.00**
Homo sapiens	F	**0.00**	0.40
Homo sapiens	M	**0.00**	0.44
Hylobates lar	F	**0.00**	**0.00**
Hylobates lar	M	**0.00**	**0.00**
Macaca cyclopis	F	**0.00**	**0.00**
Macaca cyclopis	M	**0.00**	**0.00**
Pan troglodytes	F	**0.00**	0.19
Pan troglodytes	M	**0.00**	0.16
Papio hamadryas	F	**0.00**	**0.00**
Papio hamadryas	M	**0.00**	0.28
Pongo abelii	F	**0.00**	0.89
Pongo abelii	M	**0.00**	**0.00**
Pongo pygmaeus	F	**0.00**	**0.02**
Pongo pygmaeus	M	**0.00**	**0.00**
Symphalangus syndactylus	F	**0.00**	**0.00**
Symphalangus syndactylus	M	**0.00**	**0.00**
Therapithecus gelada	F	**0.00**	**0.00**
Therapithecus gelada	M	**0.00**	0.39

Abbreviations: OTU = operational taxonomic unit; F = female; M = male.

DTAs: the first using a landmark configuration, the latter using landmarks and semi-landmarks (Fig. 4).

The average distances between the surfaces of the SM of Amud 1 and the AM Shanidar 1 amounts to 3.44 or 5.20 mm using landmarks or landmark + semi-landmarks, respectively. Using La Ferrassie 1 as the reference model, the average distances are equal to 5.87 (landmarks) and 7.06 (landmark + semi-landmarks), respectively (Fig. 7).

The main morphological differences between Amud 1 and the AM built on La Ferrassie 1 regard the occipital and zygomatic bones. As compared to Amud 1 in La Ferrassie 1, the lambda and inion landmarks appear shifted inferiorly and the zygomatic shifts backward.

The neurocranium of Amud 1 is higher and broader than in Shanidar 1, which is not surprising because Amud 1 has the largest endocranial capacity among Neanderthals. The zygomatic processes are shifted backward and the molar teeth larger than the AMs, as often reported in literature (Suzuki and Takai, 1970; Heim, 1982; Trinkaus, 2014).

DISCUSSION

Museum collections include a wealth of fossil material belonging to living and fossil primates. This material is a goldmine for understanding the evolution of this group. Unfortunately, most of it comes with the burdens (in terms of preservation quality) of diagenetic and handling accidents. This is especially true of cranial remains, which are at the same time, the most informative and (usually) the most badly deformed fossil remains. Most fossil crania are in fact broken, partially incomplete, and/or distorted. This means that crucial information is frequently lost and the general anatomy of such skulls, rather than being clearly discernible on the specimens themselves, stands largely in

TABLE 4. Correlation matrix on the Primate case study. Spearman coefficients and P-values per-formed between the phylogenetic distance expressed as number of nodes and the Procrustes distances (Table 2) and centroid size pooled by species. The values that are statistically significant are indicated in bold

Species	Sex	Phylo	*P*-value	CS	*P*-value
Alouatta caraya	F	**0.58**	**0.03**	0.52	0.06
Alouatta caraya	M	**0.67**	**0.01**	0.32	0.26
Alouatta palliata	F	0.45	0.11	**0.53**	**0.05**
Alouatta palliata	M	0.45	0.1	**0.55**	**0.04**
Ateles geoffroyi	F	0.18	0.54	**0.53**	**0.05**
Ateles geoffroyi	M	**0.3**	**0.3**	0.46	0.1
Cebus albifrons	F	**−0.21**	**0.48**	**0.55**	**0.04**
Cebus albifrons	M	−0.16	0.59	**0.53**	**0.05**
Gorilla gorilla	F	0.14	0.63	**0.59**	**0.03**
Gorilla gorilla	M	0.03	0.93	**0.66**	**0.01**
Homo sapiens	F	**0.6**	**0.02**	0.44	0.11
Homo sapiens	M	**0.55**	**0.04**	0.49	0.08
Hylobates lar	F	0.41	0.15	−0.34	0.24
Hylobates lar	M	0.49	0.08	−0.34	0.24
Macaca cyclopis	F	0.01	0.98	−0.2	0.5
Macaca cyclopis	M	0.08	0.78	−0.18	0.54
Pan troglodytes	F	−0.25	0.39	0.44	0.11
Pan troglodytes	M	0.07	0.8	0.45	0.11
Papio hamadryas	F	0.26	0.38	0.2	0.48
Papio hamadryas	M	0.2	0.49	0.05	0.86
Pongo abelii	F	0.28	0.33	**0.62**	**0.02**
Pongo abelii	M	−0.15	0.62	**0.57**	**0.03**
Pongo pygmaeus	F	0.07	0.81	**0.59**	**0.03**
Pongo pygmaeus	M	−0.05	0.88	**0.55**	**0.04**
Symphalangus syndactylus	F	0.27	0.35	−0.42	0.14
Symphalangus syndactylus	M	0.35	0.22	−0.43	0.13
Therapithecus gelada	F	0.21	0.46	0.22	0.46
Therapithecus gelada	M	0.34	0.23	0.14	0.63

Abbreviations: Phylo = phylogenetic distance; CS = centroid size; F = female; M = male.

TABLE 5. Procrustes distance calculated between: (1) starting model (SM) and manual alignments (MA); (2) disarticulated model (DM) and comparative sample; (3) SM and digital alignments (DTA). The distances referred to the specimen identified as the best aligned model are reported in bold

Procrustes distance	Specimen	Type
0.00000	Bol_2548	SM vs. SM
0.00229	VA_011	DTA vs. SM
0.00270	Bol_2529	DTA vs. SM
0.00315	VA_030	DTA vs. SM
0.00320	Bol_2548 (DM)	MA vs. SM
0.00331	OL_1192	DTA vs. SM
0.00375	Bol_2543	DTA vs. SM
0.00379	OL_1197	DTA vs. SM
0.00382	OL_1214	DTA vs. SM
0.00393	OL_1112	DTA vs. SM
0.00413	Bol_2553	DTA vs. SM
0.00428	Bol_2552	DTA vs. SM
0.00432	VA_014	DTA vs. SM
0.00437	Bol_2548 (DM)	MA vs. SM
0.00441	Bol_2545	DTA vs. SM
0.00452	Bol_2538	DTA vs. SM
0.00452	Bol_2536	DTA vs. SM
0.00466	**Bol_2546 (Tool)**	DTA vs. SM
0.00471	Bol_2532	DTA vs. SM
0.00501	Bol_2530	DTA vs. SM
0.00519	OL_1068	DTA vs. SM
0.00520	VA_022	DTA vs. SM
0.00529	Bol_2541	DTA vs. SM
0.00549	Bol_2535	DTA vs. SM
0.00564	Bol_2537	DTA vs. SM
0.00566	Bol_2531	DTA vs. SM
0.00574	Bol_2550	DTA vs. SM
0.00578	OL_0794	DTA vs. SM
0.00586	VA_020	DTA vs. SM
0.00587	Bol_2542	DTA vs. SM
0.00597	Bol_2540	DTA vs. SM
0.00611	OL_1428	DTA vs. SM
0.00613	OL_1193	DTA vs. SM
0.00640	OL_0886	DTA vs. SM
0.00651	Bol_2525	DTA vs. SM
0.00658	Bol_2524	DTA vs. SM
0.00660	Bol_2527	DTA vs. SM
0.00684	VA_029	DTA vs. SM
0.00708	Bol_2533	DTA vs. SM
0.00711	Bol_2551	DTA vs. SM
0.00720	**Bol_2546 (Tool)**	DTA
0.00724	Bol_2548 (DM)	MA vs. SM
0.00748	OL_1282	DTA vs. SM
0.00749	OL_0866	DTA vs. SM
0.00755	Bol_2540	DTA
0.00758	Bol_2542	DTA
0.00766	Bol_2531	DTA
0.00767	Bol_2527	DTA
0.00776	OL_0869	DTA vs. SM
0.00786	Bol_2529	DTA
0.00806	Bol_2530	DTA
0.00826	OL_1199	DTA vs. SM
0.00836	Bol_2547	DTA vs. SM
0.00859	Bol_2552	DTA
0.00865	Bol_2543	DTA
0.00867	Bol_2548 (DM)	MA vs. SM
0.00879	Bol_2553	DTA
0.00879	OL_1187	DTA vs. SM
0.00880	Bol_2532	DTA
0.00898	Bol_2528	DTA
0.00901	Bol_2541	DTA
0.00902	Bol_2538	DTA
0.00916	Bol_2550	DTA
0.00925	Bol_2525	DTA
0.00940	Bol_2537	DTA
0.00949	Bol_2545	DTA
0.00957	Bol_2544	DTA vs. SM
0.00958	VA_013	DTA vs. SM
0.00964	Bol_2524	DTA
0.00966	Bol_2536	DTA
0.00998	VA_033	DTA vs. SM
0.01016	Bol_2544	DTA
0.01042	Bol_2551	DTA
0.01070	Bol_2539	DTA vs. SM
0.01099	Bol_2547	DTA
0.01099	VA_031	DTA vs. SM
0.01108	Bol_2548 (DM)	MA vs. SM
0.01109	Bol_2535	DTA
0.01111	Bol_2533	DTA
0.01138	Bol_2539	DTA
0.01158	Bol_2526	DTA vs. SM
0.01212	Bol_2526	DTA
0.01212	Bol_2548 (DM)	MA vs. SM
0.01370	Bol_2548 (DM)	MA vs. SM
0.01396	Bol_2528	DTA vs. SM
0.01404	Bol_2548 (DM)	MA vs. SM
0.01465	Bol_2548 (DM)	MA vs. SM
0.01544	Bol_2548 (DM)	MA vs. SM
0.01752	Bol_2548 (DM)	MA vs. SM
0.04986	VA_011	DTA
0.05373	OL_1282	DTA
0.05476	OL_1197	DTA
0.05664	OL_1199	DTA
0.05993	VA_029	DTA
0.05997	OL_0866	DTA
0.06039	VA_031	DTA
0.06064	VA_033	DTA
0.06078	OL_1428	DTA
0.06157	OL_1112	DTA
0.06208	VA_022	DTA
0.06257	OL_1068	DTA
0.06425	OL_1193	DTA
0.06434	OL_1192	DTA
0.06516	OL_0869	DTA
0.06729	OL_1187	DTA
0.07142	VA_013	DTA
0.07168	OL_1214	DTA
0.07233	OL_0886	DTA
0.07274	VA_014	DTA
0.07314	VA_020	DTA
0.07337	VA_030	DTA
0.07933	OL_0794	DTA

the minds of observers. Manual reconstructions have always provided invaluable assistance in the case of deformed or broken specimens. Yet, they rest on the ability and subjective judgment of a few highly trained operators, which is time consuming, prone to errors (MacLeod et al., 2010; Boyer et al., 2015) and comes in limited availability. Fortunately, a growing number of virtual procedures, based on digital reconstructions of the remains, now allow the restoration of original shapes of the fossil specimens.

Here, we propose a new landmark-based method, DTA, to align disarticulated parts belonging to the same specimen, and applied DTA on three different case studies. The first involves a large sample of extant primates and

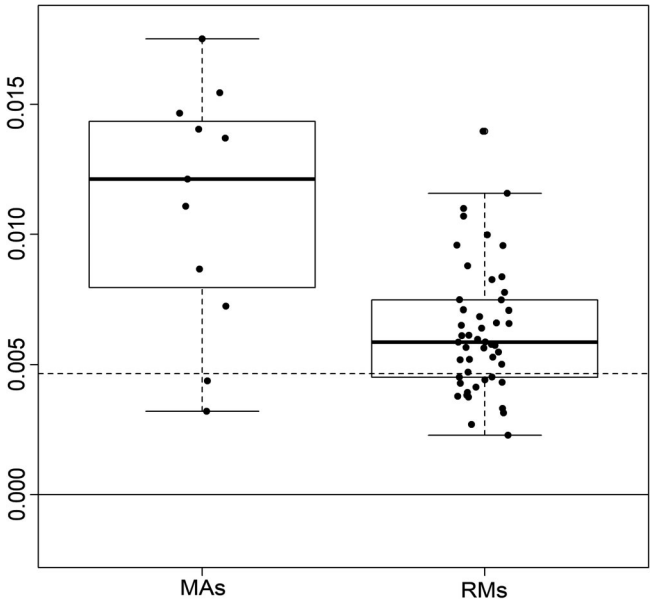

Fig. 5. Boxplot of the Procrustes distances calculated between the landmark configuration sampled on the original 3D model used as case study (continue line), the manual alignments (MAs), the landmark configurations obtained aligning the two halves on a comparison sample (RMs), and the digital alignment performed by the tool (dashed line). The differences between the means of the groups MAs and RMs are statistically different (*P*-value <0.001). Abbreviations: MAs = manual alignments; RMs = aligned reference models.

provides an exhaustive application with more than 3,600 DTAs being carried out. This made it possible to quantify DTA performance, and assess the importance of sex, size, and taxonomic identity in providing the best reference model in guiding the alignments. We found DTA performance is influenced by taxonomic affiliation, sex, and CS. In particular, the individual within the RM set often coincide with the species identity, sex, and size of the target. Hence, phylogenetic and allometric effects, together with sex differences, play a crucial role into identifying the appropriate reference model for DTA. However, a large RM set always grants DTA will find an ideal reference model to properly reconstruct the target shape.

We directly compared DTA to manual alignments in our second case study, a *Homo sapiens* skull broken in two halves. DTA performs better than manual alignments on average. However, there are a minority of manual alignments that work better. These results suggest that DTA works almost as well as expert-based reconstruction, which is fundamental in situations where the handling of fossil items is difficult, dangerous (because the specimen is delicate), or simply unavailable. This is especially true of rare, exceptionally important fossils such as BOU-VP-12/130 (*Australopithecus garhi*) (Asfaw et al., 1999), AL-442 (*Australopithecus afarensis*) (Kimbel et al., 2004), OH5 (*Paranthropus boisei*) (Leakey, 1959; Benazzi et al., 2011), ATD6-15 and ATD6-69 (*Homo antecessor*) (De Castro et al., 1997), Amud 1 (*Homo neanderthalensis*) (Suzuki and Takai, 1970; Amano et al., 2015), Le Moustier 1 (*Homo neanderthalensis*) (Klaatsch and Hauser, 1909; Thompson and Illerhaus, 1998; Ponce De León and Zollikofer, 1999; Ponce De León, 2002), and the Neanderthal infant from Mezmaiskaya (Gunz et al., 2012).

Our third case study used DTA on the Amud 1 Neandertal skull. This alignment is complicated by the fact that the two cranial portions of the skull are not contiguous, leaving a large gap of missing bone below the orbits and around the nasal cavity. The independent, expert-based restoration

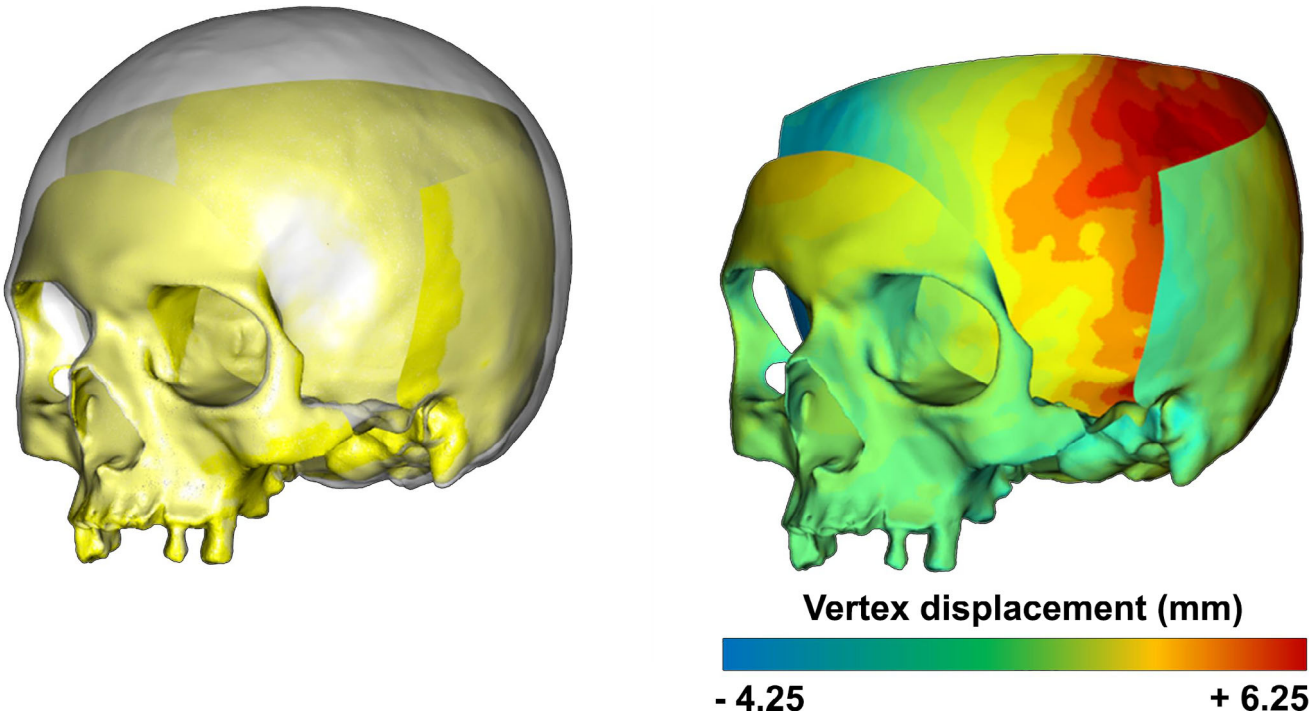

Fig. 6. DTA applied on *Homo sapiens* case study. On the left, the AM after DTA (yellow) and the starting model (white). On the right, the vertex displacement showed on the AM. Abbreviations: DTA = Digital Alignment Tool; AM = aligned model.

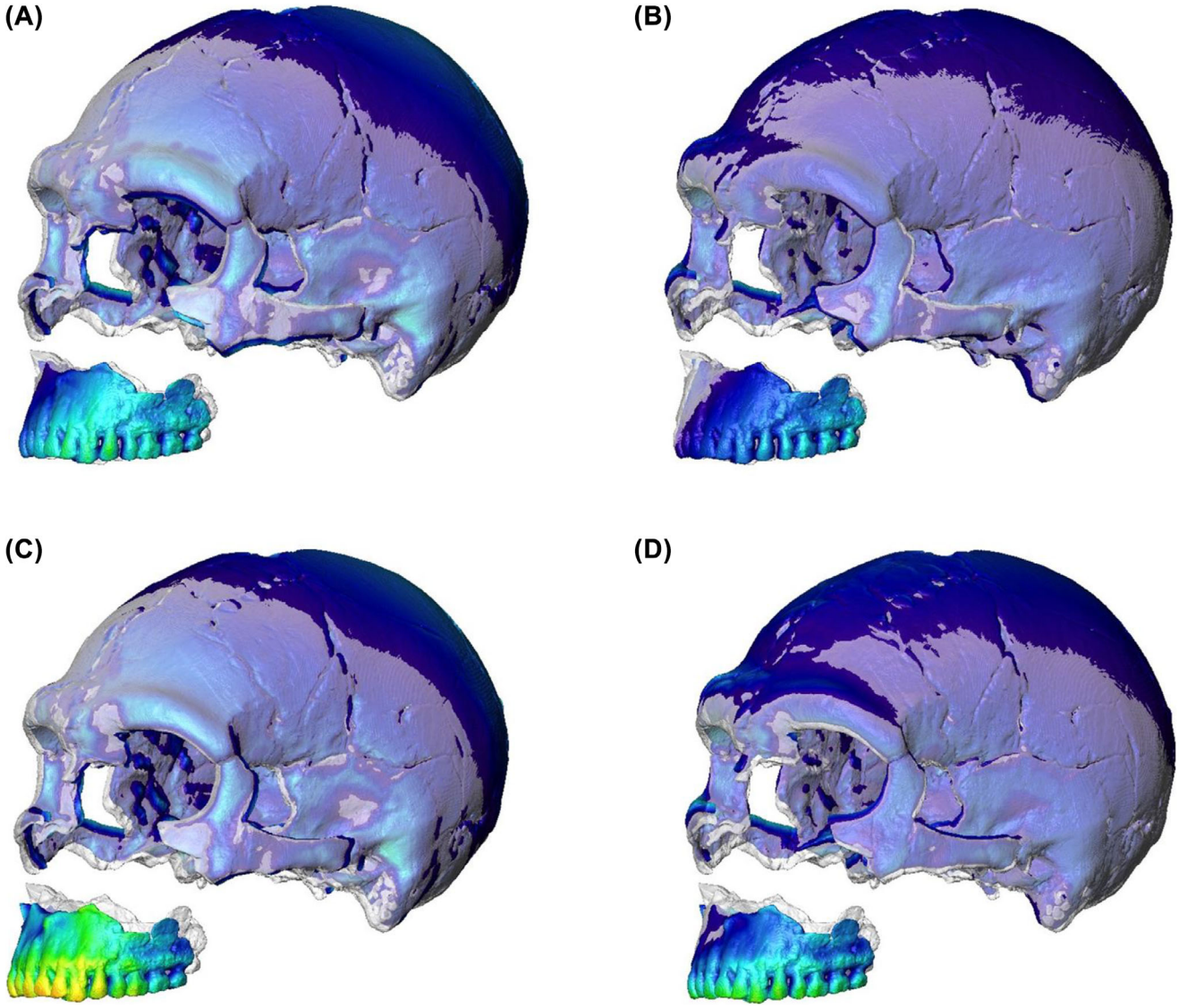

Fig. 7. DTA applied on Amud 1 using respectively La Ferrassie 1 (**A**, **C**) and Shanidar 1 (**B**, **D**) as reference. DTA was applied using landmark (A, B) and landmark + semi-landmarks (C, D). Abbreviations: DTA = Digital Alignment Tool.

(Suzuki and Takai, 1970) we used to verify our digital alignment is a mere 3 mm different from the DTA product. These results confirm the usefulness of DTA as a technique for aligning broken fossil specimens and accessing the three-dimensional shape of otherwise troublesome, hard to access material, while also providing the fine details which digital models make available. As compared to other tools enabling the morphological analysis of 3D articulated structures (e.g., Vidal-Garcia et al., 2017), DTA is more flexible and not constrained to rigid rotations.

In virtual anthropology, most reconstructions use a collection of living primate skulls as a reference. Building a sound reference sample can be difficult when conspecifics of the same age and sex are not available or otherwise easily identifiable. For example, in 2009, Gunz and colleagues reconstructed the Taung child (*Australopithecus africanus*) by TPS warping using a juvenile chimpanzee cranium as the RM (Gunz et al., 2009). Although conceivable, this was not necessarily the best option for the fossil reconstruction. The DTA procedure proposed here allows the user to select the closest specimen to the target minimizing bias in the virtual restoration procedure, thus bypassing the need for using a subjectively chosen RM which could be severely misleading.

The results of the primate case study highlight how critical, and tricky, the choice of the RM could be. Contrary to expectation, specimens of close phylogenetic affinity are not always the best choice. Allometric factors or convergence, such as in the case of the highly specialized vocal tracts in *Pongo* and *Alouatta* (Biegert, 1963; Shea, 1985; Profico et al., 2017; Fiorenza and Bruner, 2018) may in fact influence cranial morphology and show how challenging the choice of an appropriate RM can be. Even when a large comparative sample of the same species as the DM is available (as in our *Homo sapiens* case study), the performance of the DTA varies greatly across RMs, suggesting that allometric and sex effects are always highly influential.

A few generalizations emerge from this study, which introduces a new and powerful tool for the alignment of disarticulated cranial material. First, when available, it is appropriate to use a specimen belonging to the same species and sex of the disarticulated model as the RM. Although DTA could be used to select the RM, this must be taken into consideration when confronting a limited number of reference items. Second, although manual restorations of the original shapes of fossil skulls are often highly accurate, this study demonstrates that DTA is at least as precise and accurate as manual alignments but gives the advantages of being cheaper, faster, and providing unrestrained access to the aligned digital model. The alignment of Amud 1, which differs by only 3 mm from the original restoration, demonstrates the utility and accuracy of DTA on a real case study from the human fossil record and the potential importance of DTA for use in future studies of fragmented fossil crania.

ACKNOWLEDGMENTS

We thank the Smithsonian Institution (www.vertebrates.si.edu), the Kyoto University Primate Museum (www.dmm.pri.kyoto-u.ac.jp), the anthropological Museum "G. Sergi" (Rome, Italy), the Museo Nacional de Ciencias Naturales, Universidad Complutense de Madrid (Oloriz collection), and the online databases of NESPOS (www.nespos.org) and Morphosource (www.morphosource.org) for kindly providing their osteological database. We are grateful to prof. Israel Hershkovitz and dr. Julia Abramov for access to the 3D model of Amud 1. We thank Emiliano Bruner for his kind comments and suggestions. We also thank 11 anonymous operators for the manual alignments performing.

LITERATURE CITED

Amano H, Kikuchi T, Morita Y, Kondo O, Suzuki H, Ponce de León MS, Zollikofer CPE, Bastir M, Stringer C, Ogihara N. 2015. Virtual reconstruction of the Neanderthal Amud 1 cranium. Am J Phys Anthropol 158:185–197.

Arbour JH, Brown CM. 2013. Incomplete specimens in geometric morphometrics analyses. Methods Ecol Evol 5(1):16–26.

Arbour VM, Currie PJ. 2012. Analyzing taphonomic deformation of ankylosaur skulls using retrodeformation and finite element analysis. PLoS One 7:e39323.

Arnold C, Matthews LJ, Nunn CL. 2010. The 10kTrees website: a new online resource for primate phylogeny. Evol Anthropol 19:114–118.

Asfaw B, White T, Lovejoy O, Latimer B, Simpson S, Suwa G. 1999. Australopithecus garhi: a new species of early hominid from Ethiopia. Science 284:629–635.

Benazzi S, Bookstein FL, Strait DS, Weber GW. 2011. A new OH5 reconstruction with an assessment of its uncertainty. J Hum Evol 61:75–88.

Benazzi S, Gruppioni G, Strait DS, Hublin J. 2014. Technical Note: Virtual reconstruction of KNM-ER 1813 Homo habilis cranium. Am J Phys Anthropol 153:154–160.

Biegert J. 1963. The evaluation of characteristics of the skull, hands and feet for primate taxonomy. Classif Hum Evol 37:116–145.

Boyer DM, Puente J, Gladman JT, Glynn C, Mukherjee S, Yapuncich GS, Daubechies I. 2015. A new fully automated approach for aligning and comparing shapes. Anat Rec 298:249–276.

De Castro JMB, Arsuaga JL, Carbonell E, Rosas A, Martìnez I, Mosquera M. 1997. A hominid from the lower Pleistocene of Atapuerca, Spain: possible ancestor to Neandertals and modern humans. Science 276:1392–1395.

Di Vincenzo F, Profico A, Bernardini F, Cerroni V, Dreossi D, Schlager S, Zaio P, Benazzi S, Biddittu I, Rubini M. 2017. Digital reconstruction of the Ceprano calvarium (Italy), and implications for its interpretation. Sci Rep 7:13974.

Fiorenza L, Bruner E. 2018. Cranial shape variation in adult howler monkeys (*Alouatta seniculus*). Am J Primatol 80:e227729.

Gunz P, Mitteroecker P, Neubauer S, Weber GW, Bookstein FL. 2009. Principles for the virtual reconstruction of hominin crania. J Hum Evol 57:48–62.

Gunz P, Neubauer S, Golovanova L, Doronichev V, Maureille B, Hublin J-J. 2012. A uniquely modern human pattern of endocranial development. Insights from a new cranial reconstruction of the Neandertal newborn from Mezmaiskaya. J Hum Evol 62:300–313.

Heim JL. 1982. *Les hommes fossiles de La Ferrassie*, Vol. 2. Masson, Paris.

Hughes NC, Jell PA. 1992. A statistical/computer-graphic technique for assessing variation in tectonically deformed fossils and its application to Cambrian trilobites from Kashmir. Lethaia 25:317–330.

Kimbel WH, Rak Y, Johanson DC. 2004. *The skull of Australopithecus afarensis*. New York: Oxford University Press.

Klaatsch H, Hauser O. 1909. *Homo mousteriensis Hauseri: ein altdiluvialer Skelettfund im Departement Dordogne und seine Zugehörigkeit zum Neandertaltypus*. Friederich Vieweg und Sohn. Arch Anthropol (new series) 7:287–297.

Leakey LSB. 1959. A new fossil skull from Olduvai. Nature 184: 491–493.

Lyman RL. 1994. *Vertebrate taphonomy*. New York: Cambridge University Press.

MacLeod N, Benfield M, Culverhouse P. 2010. Time to automate identification. Nature 467:154–155.

Ogihara N, Nakatsukasa M, Nakano Y, Ishida H. 2006. Computerized restoration of nonhomogeneous deformation of a fossil cranium based on bilateral symmetry. Am J Phys Anthropol 130:1–9.

Ponce De León MS. 2002. Computerized paleoanthropology and Neanderthals: The case of Le Moustier 1. Evol Anthropol 11:68–72.

Ponce De León MS, Zollikofer CPE. 1999. New evidence from Le Moustier 1: computer-assisted reconstruction and morphometry of the skull. Anat Rec 254:474–489.

Profico A, Bellucci L, Buzi C, Di Vincenzo F, Micarelli I, Strani F, Tafuri MA, Manzi G. 2018a. Virtual anthropology and its application in cultural heritage studies. Stud Conserv 1–14. https://doi.org/10.1080/00393630.2018.1507705. In Press.

Profico A, Piras P, Buzi C, Di Vincenzo F, Lattarini F, Melchionna M, Veneziano A, Raia P, Manzi G. 2017. The evolution of cranial base and face in Cercopithecoidea and Hominoidea: modularity and morphological integration. Am J Primatol 79:e22721.

Profico A, Veneziano A, Melchionna M, Piras P, Raia P. 2018b. *Arothron: R functions for geometric morphometrics analyses*. https://doi.org/10.5281/zenodo.1243073.

Schlager S, Profico A, Di Vincenzo F, Manzi G. 2018. Retrodeformation of fossil specimens based on 3D bilateral semi-landmarks: implementation in the R package "Morpho.". PLoS One 13:e0194073.

Shea BT. 1985. On aspects of skull form in African apes and orangutans, with implications for hominoid evolution. Am J Phys Anthropol 68:329–342.

Shipman P. 1981. *Life history of a fossil and introduction to taphonomy and paleoecology*. Cambridge: Harvard University Press.

Suzuki H, Takai F. 1970. *The Amud man and his cave site*. Tokio: Academic Press of Japan.

Tallman M, Amenta N, Delson E, Frost SR, Ghosh D, Klukkert ZS, Morrow A, Sawyer GJ. 2014. Evaluation of a new method of fossil retrodeformation by algorithmic symmetrization: crania of papionins (primates, Cercopithecidae) as a test case. PLoS One 9:e100833.

Thompson JL, Illerhaus B. 1998. A new reconstruction of the Le Moustier 1 skull and investigation of internal structures using 3-D-Î¼CT data. J Hum Evol 35:647–665.

Trinkaus E. 2014. *The shanidar neandertals*. New York: Academic Press.

Vidal-Garcia M, Bandara L, Keogh JS. 2017. ShapeRotator: an R package for standardised rigid rotations of articulated three-dimensional structures with application for geometric morphometrics. bioRxiv:159392.

Zollikofer CPE, de León MSP, Lieberman DE, Guy F, Pilbeam D, Likius A, Mackaye HT, Vignaud P, Brunet M. 2005. Virtual cranial reconstruction of Sahelanthropus tchadensis. Nature 434:755–759.